One-step synthesis of highly pure and well-crystallized vertically aligned carbon nanotubes

Emeline Charon, Mathieu Pinault, Martine Mayne-L'Hermite, Cécile Reynaud

One-step synthesis of highly pure and well-crystallized vertically aligned carbon nanotubes

Emeline Charon*, Mathieu Pinault, Martine Mayne-L'Hermite, Cécile Reynaud

Université Paris-Saclay, CEA, CNRS, NIMBE, 91191 Gif sur Yvette Cedex, France

* Corresponding author. Tel: 33 1 69 08 53 05. E-mail: emeline.charon@cea.fr

Abstract (197 words)

The one-step aerosol-assisted catalytic chemical vapor deposition (CCVD) process, when operated in a H_2-based carrier gas, is shown to be effective at an extremely low ferrocene content (0.1wt.% in toluene), which enables to efficiently prepare forests of vertically aligned multiwalled carbon nanotubes (VACNTs) with high purity and good crystalline level. The resulting iron content in VACNT sample is only 0.5wt.% corresponding to a high catalytic yield of 200 while the steady growth rate (20 µm/min) is maintained at a significant value. The iron content in the sample is found proportional to the ferrocene concentration in the precursor, and when it decreases, a noticeable reduction in the iron encapsulation frequency in the nanotube channel is plainly observed. Lowering the ferrocene concentration generates a reduction in the VACNT number density while the growth rate increases and CNT diameters and crystalline structure remain similar. Such significant purity and crystalline levels involves a high oxidation resistance of the VACNT forest. These results, together with the *in-situ* continuous growth feature of the one-step aerosol assisted CCVD process, open up towards a new VACNT range made of pure and well-crystallized multi-walled carbon nanotubes, which is of interest for industrial production and commercial applications.

Keywords: vertically aligned carbon nanotubes; one-step catalytic chemical vapour deposition; iron content; purity; crystallinity; oxidation resistance.

1 Introduction

Vertically Aligned Carbon NanoTubes (VACNT) arrays have demonstrated outstanding potentialities as a novel material to prepare nanostructured composite or multifunctional materials. The carbon nanotube (CNT) alignment allows to take advantage of their anisotropic properties. This is useful for many applications of high societal interest such as heat transfer [1], energy storage [2,3], or high performance structural composites [4,5]. Efforts are currently underway to develop efficient synthesis processes for the manufacture of VACNTs in order to achieve mass production while reducing costs [6,7]. In particular, the process must be as simple as possible and must be operated at atmospheric pressure. The most effective method for synthesizing VACNT is catalytic chemical vapor deposition (CCVD) [8] which can be operated at atmospheric pressure. However, it often involved several preliminary steps at low pressure to prepare the layer of catalytic nanoparticles from which the nanotubes will then grow. It is why the aerosol-assisted version of the CCVD process has been developed [9–14], where catalyst nanoparticles are produced in situ and continuously refreshed due to the simultaneous injection of both metal and carbon precursors[15]. This process involves a base-growth mechanism [16] enabling the continuous growth of VACNTs at steady growth rate over very long synthesis duration, which allows VACNTs greater than 1mm to be achieved. Therefore, aerosol-assisted CCVD is a versatile, cost-effective and scalable one-step process operated at atmospheric pressure potentially applicable for a roll to roll production of multi-walled VACNTs. The continuous supply of ferrocene, which is essential to sustain the growth through the refreshment of the catalyst nanoparticles [16], induces the encapsulation of short nanowires in the inner channel of the nanotubes [17,18]. As a consequence, the iron content of the pristine VACNTs (Table 1) is typically around a few wt.% [15,19–21]. Such metallic by-products can alter the intrinsic nanotube properties and be detrimental for several applications [22]. In addition, it is also recognized that they can catalyze the oxidation of nanotubes and thus affect their stability in air at moderate temperatures [23–25]. Therefore, these CNTs need to be purified and several methods have been developed to remove metal by-products [22], either by acid treatment [26], but their complete removal is difficult to achieve without altering the nanotube structure [27,28], or by high temperature annealing which is the most effective method for their removal while improving the nanotube crystallinity [22,29,30]. However, such treatments complicate the CNT production process and are not always compatible with the targeted application.

Therefore, efforts must be done directly on the aerosol-assisted CCVD production process in order to reduce drastically the iron content in the pristine VACNTs. Recently and in the meantime of our study, this issue was addressed by T. Kinoshita *et al.* [31] who reported a modified floating catalyst CCVD method (similar to the aerosol-assisted one) enabling the growth of CNT forests containing very low concentration of impurity (0.8 wt%). However, the changes made to the process have turned it into a two-step process involving in the first step the in-situ formation of the catalyst particles, then in the second step the CNT growth with carbon precursors only. Such experimental conditions do not allow the refreshment of the catalyst particles so that the lifetime of their process is limited. Moreover the second step was performed at low pressure which limits the industrial interest of the method.

In this context, the aim of our work is to reduce the Fe content of pristine VACNTs while preserving their crystallinity, alignment and growth rate by increasing the catalytic yield of the one-step aerosol-assisted CCVD process operated at atmospheric pressure. In the literature (Table 1), few studies [15,19–21] report the measurement of iron content of VACNTs formed by the one-step aerosol-assisted CCVD, but it is generally found that iron content increases with ferrocene concentration in the precursor solution [19,21]. Cho *et al*. [20] studied the [0.2-9] wt.% ferrocene range at 760°C and obtained 1.9wt.% as the lowest iron content in CNT samples for 1.5wt.% of ferrocene in toluene. However, they did not observe any growth of VACNT forests at 0.2wt.% of ferrocene, in agreement with the result of Singh *et al*. [13]. Similarly, Castro *et al.* [15] observed no growth of VACNT at 0.1 and 0.5wt.% when studying the [0.1-5] wt.% range of ferrocene at 850°C and the lowest iron content obtained is 3wt.% at 2.5wt% ferrocene with a higher growth rate due to a higher synthesis temperature. To our knowledge, for one-step aerosol-assisted CCVD process, the lowest concentration of ferrocene responsible for the growth of VACNTs is 0.1wt.% [32] but the growth rate at 750°C is particularly low (0.4 µm/min) and the iron content in the resulting sample is not reported. The highest growth rate obtained with a low ferrocene concentration (0.58wt.%) is 13.6 µm/min at 780°C [33] but the iron content is not indicated. The latter result was obtained with 15% H_2 added to Ar as carrier gas.

Table 1 : Lowest ferrocene concentrations giving rise to VACNT growth reported in the literature for the one-step aerosol-assisted CCVD synthesis. The most relevant experimental parameters are reported, as well as, the growth rate and iron content of the final product when available. Ferrocene concentrations in the precursor solution were converted to wt.%. Note that 1wt.% of ferrocene in toluene corresponds to a Fe/C ratio of 0.07at.%.

	Ferrocene concentration (wt.%)	Carbon source	Carrier gas	T (°C)	Substrate	Growth rate (µm/min)	Iron content (wt.%)	**Raman ID/IG λ (nm)**
Bai 2005 [33]	0.58	xylene	Ar/H_2 87/13	780	quartz	13.6	-	-
	1.14					20.4		-
Ionescu 2011 [32]	0.1	xylene	Ar	750	Sputtered Al Si wafer	0.4	-	0.49 785 nm
	1					4.7		0.68 785 nm
Cho 2012 [20]	1.5	toluene	Ar	760	quartz	2.5	1.9	0.33* 633 nm
McKee 2009 [19]	0.54	benzene	Ar	750	various	-	0.7 - 3	0.3 measured at 1.75 wt% Fe 514 nm
Meysami 2013 [21]	1	toluene	Ar	800	quartz	16	2.5	0.29 532 nm
Castro 2010 [15]	1.25	toluene	Ar	850	quartz	11	3.5	0.52* 532 nm
	2.5					20	3	0.33* 532 nm
Castro 2013 [34]	2.5	toluene	Ar/H_2 80/20	850	quartz	29	5.3	-
				800		23	6.2	-

* Area ratio

Despite the wide disparity in the experimental conditions, the results of the literature highlight the important role played by the synthesis temperature and the hydrogen presence in the carrier gas to maintain a realistic growth rate while decreasing the ferrocene concentration in the aerosol. In a previous paper [34], we studied the effect of adding hydrogen to Ar carrier gas and showed that it has a major impact on the aerosol-assisted CCVD process. Increasing the hydrogen content strongly shifts the CNT growth to the reactor inlet and reduces the CNT diameters, while the CNT number density increases. Indeed, hydrogen demonstrably affects the

gas phase phenomena by lowering the decomposition temperature of ferrocene, promoting the formation of a larger number of smaller iron nanoparticles in the gas phase and increasing the nucleation site density of the catalytic nanoparticles. In addition, the optimal synthesis temperature in terms of yield and homogeneity of growth is reduced to 800°C under hydrogen (Table 1) [34]. In these previous experiments, the concentration of ferrocene in toluene was set at 2.5wt.%, the optimal concentration determined at 850°C without H_2 [15]. It should be reminded that without H_2, no growth of VACNTs is obtained below 1.25wt.% of ferrocene, neither at 850°C nor at 800°C. However, the situation may change in the presence of H_2 due to the significant improvement in the ferrocene decomposition it induces. Therefore, our objective is to determine, in the presence of H_2, the lowest concentration of ferrocene in toluene allowing the growth of a VACNT forest with low impurity level while maintaining a high growth rate and a good structural quality.

In this paper, we investigate the role of ferrocene concentration in the precursor solution (toluene/ferrocene) on the VACNT growth and characteristics (iron content, length, diameter, density, structure, oxidation resistance as well as on growth efficiency (yields and growth rate). As hydrogen was reported to be a determining chemical player in the decomposition rate of ferrocene [34], all the synthesis of this study are performed by the one-step aerosol assisted CCVD process with hydrogen diluted in argon as carrier gas. The approach combines global analysis by Scanning Electron Microscopy (SEM), Thermogravimetric Analysis (TGA) and Raman Spectrometry, with local analysis by Transmission Electron Microscopy (TEM). Since in this one-step aerosol assisted CCVD process a continuous supply of ferrocene is essential to sustain growth [35], our first objective is to determine the ferrocene concentration threshold above which VACNT growth is maintained once the catalytic particles are formed. To this end, we first carry out double injection experiments, by designing a specific set-up allowing to use a solution containing 2.5wt.% ferrocene in a first short injection sequence to form the catalyst particles, and then to use a second solution with a lower ferrocene concentration in a second long injection sequence. These experiments demonstrate that a very low ferrocene concentration (0.01wt.%) used in the second sequence can sustain the growth of VACNT forest, which is considerably lower than the ones reported in the literature for this one-step aerosol assisted CCVD process. Subsequently, by operating this process in a single injection mode with a ferrocene concentration decreasing from 2.5 to 0.01wt.%, we show that it is possible to determine conditions to synthesize a pristine VACNT carpet with unprecedented reported low iron content (0.5 wt%) and high oxidation resistance.

2 Experimental

2.1 Synthesis

The set-up (Fig. 1) and standard procedure used to synthesize VACNTs by the one-step aerosol-assisted CCVD process at atmospheric pressure are similar to those described by Castro *et al.* [34]. Note that syntheses in the presence of H_2 cannot be done under the same conditions as in its absence because the addition of H_2 considerably shifts the VACNT growth towards the reactor inlet. The synthesis temperature must then be lowered to restore growth in the reactor center. This is why all syntheses here are made in the presence of H_2 and at the optimal temperature of 800°C [34]. The furnace exhibits an isothermal area larger than the previous one. It is a 45 cm long tubular furnace equipped with a quartz reactor (16 mm inner diameter). At 800°C, the isothermal area (±10°C), is extended from 10 to 35 cm from the furnace inlet (Fig. 1). A flat quartz substrate of 1.5x0.75 cm^2 is placed in the isothermal area at 14 cm from the reactor inlet. The VACNTs grown on this substrate are analyzed together with the VACNTs grown on the reactor walls. The VACNTs grown on the reactor walls are collected with a stainless scraper, a procedure which keeps intact their morphology and structure. They are weighed according to the location in the reactor, divided into 5 cm long sections with a surface area of 25 cm^2 each, in order to assess the distribution of the VACNT deposit. All the characterizations will be carried out on the VACNTs coming from the substrate of zone 2 and the VACNT powder coming from zone 3. These zones were chosen because the yield is better there. To perform double injection experiments, the present set-up is equipped with two liquid precursor tanks. Solutions of ferrocene dissolved in toluene at different concentrations are poured into these tanks connected to an injection system and an evaporator where they are nebulized and carried to the reactor by a gas flow of 1 L/min at a rate about 0.8 g/min. The gas flow is a mixture of Ar and 30 vol.% of H_2. A solution with 2.5wt.% of ferrocene is poured into tank A (Fig. 1) while in tank B, the solution has variable concentrations. The solution in tank A is injected for 1 min 40 s and then the solution in tank B for 13 min 20 s. The switch from tank A to tank B is instantaneous, so that the process remains a one-step continuous process. In single injection experiments, only the solution in tank B is injected for 15 min, with ferrocene concentrations ranging from 0.01 to 2.5wt.%.

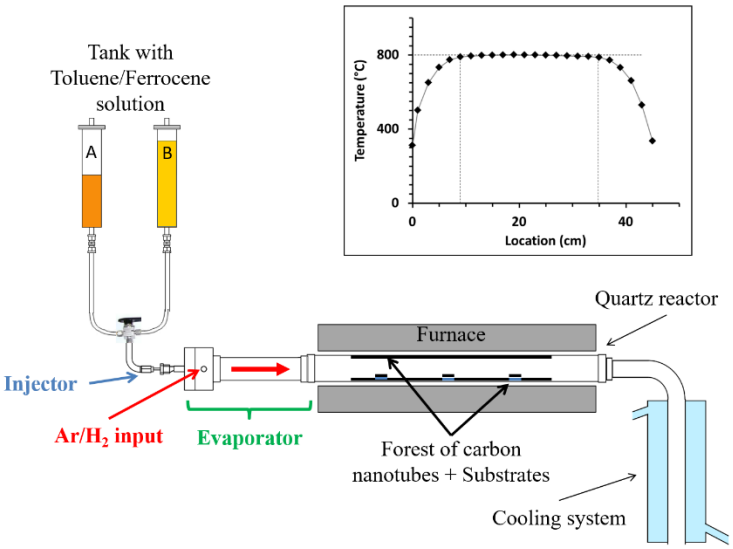

Fig. 1: Experimental set-up used for the one-step aerosol-assisted CCVD process operated at atmospheric pressure. Insert: temperature profile at 800°C measured with a thermocouple moved along the quartz reactor.

2.2 Characterizations

Morphology and thickness of VACNT carpets grown on the substrate and on the walls in the center of the reactor are investigated by SEM (Carl Zeiss Ultra 55). CNT structure and statistical analysis of external and internal diameters are obtained from TEM (Philips CM12, 120 kV) after ultrasonic dispersion of CNTs in ethanol and deposition on standard TEM holder (copper grids). For high resolution TEM, we use a JEOL 2011 operating at 200 kV, equipped with a CCD camera (GATAN system ORIUS SC100, 4008×2672 pixels, pixel size: 0.014 nm).

TGA under air of products collected in the area in the center of the reactor is performed with a 92–16.18 SETARAM apparatus, at a temperature rate of 10°C/min in the 20-1000°C range, which leads to the complete gasification of carbon. The rusty residue is used to determine the iron content of the sample (weight percentage of iron in the collected products), as well as the catalytic yield (ratio between the carbon and iron masses). This iron content is calculated knowing that the residue consists of Fe_2O_3 as shown by X-ray diffraction [36]. In the unlikely event that FeO contributes to the residue, the error would be small since the mass of iron in Fe_2O_3 is 70%, while it is 78% in FeO. We will see in the following that this error would be negligible given the magnitude of the variation in iron content in our experiments.

Raman spectra are acquired from the substrate samples in ambient conditions using a Renishaw INVIA microspectrometer equipped with an Ar laser (514.5 nm wavelength), focused through a Leica microscope. A very low incident power (2 mW) is used to avoid heating effects. Spectra

are recorded in the middle of the carpet cross-section in the 1000-3500 cm^{-1} range. Pertinent quantitative Raman parameters are obtained by conventional fitting procedures [37] for the classical G, D, D' and 2D bands [38] and the corresponding position, full-width at half maximum (FWHM) and intensity (band height) relative to the G band are reported in Table S1 (Supplementary data).

3 Results

3.1 Thickness and growth rate of the VACNT forests

Double injection experiments

Double injection syntheses are performed with a first injection sequence with 2.5wt.% ferrocene in toluene during 1 min 40 s immediately followed by a long injection sequence of 13 min 20 s with a ferrocene concentration varying between 0.01 and 1.5wt.%. In preliminary experiments, we checked that the 1 min 40 s duration is long enough to initiate a VACNT carpet representative of a VACNT growth with a ferrocene concentration of 2.5wt.% (See Fig. S1 in supplementary data). SEM images of the products grown on quartz substrates placed in the oven center (Fig. 2a) reveal VACNT forests of the same good quality as usually reported [34]. The shortest carpet (170 µm) is obtained for 0.01wt.% of ferrocene in the second injection sequence, but then, the thickness increases sharply to 330 µm for 0.05wt.% and up to 380 µm for 0.1wt.%, after which it remains around 270 µm for higher concentrations. The corresponding growth rate (Fig. 2b) exceeds 25 µm/min at 0.1wt.% of ferrocene and stabilizes between 15 and 20 µm/min at higher concentrations.

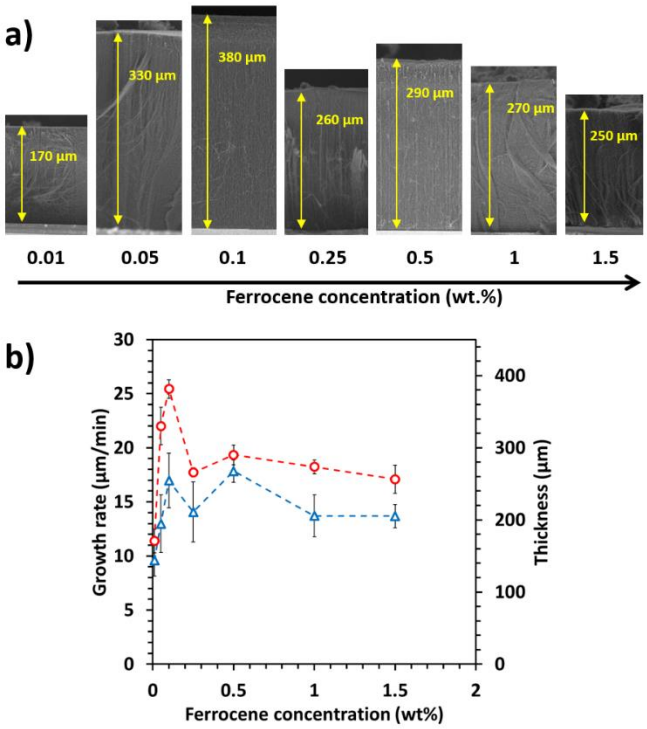

Fig. 2: Double injection. (a): SEM images of the VACNT carpets grown on the central substrate (side-view) for increasing ferrocene concentration in the second long injection sequence. (b): mean carpet thickness and growth rate on the substrate (red dot) and on the reactor walls (blue triangle) as a function of ferrocene concentration. Dashed lines are added as eyes guide only. The thickness distribution was measured by SEM on the same samples with 20 measurement points for the CNTs on the walls of the reactor and 3 measurement points for the CNTs on the substrate.

The values on the substrate are slightly higher than those obtained on samples collected on the reactor walls. (Fig. 2b). It is because the substrate is placed upstream along the reactor of the zone where the samples used for the SEM analysis are collected and that, in aerosol-assisted CCVD, the growth yield decreases along the reactor due to the dynamics of the catalytic nanoparticles deposition as observed previously by us [15,34] and others [36]. This effect is confirmed by the measurement of the mass distribution along the reactor displayed in Fig.S2. As detailed in Supplementary Data, Fig.S2 shows that, whatever the ferrocene concentration, the yield is optimal in zone 2 where the substrate is placed while the collected zone considered in Fig.2 is zone 3 where the yield is slightly lower.

The most striking result of these double injection experiments is that, in the presence of H_2, a ferrocene concentration as low as 0.01wt.% in the second injection sequence is sufficient to sustain the growth, and a rate higher than 15 µm/min is obtained for a concentration from 0.05wt.%.

Single injection experiments

Considering the very low ferrocene concentration (0.01 wt%) able to sustain the growth in double injection synthesis, single injection synthesis with ferrocene concentration from 0.01 to 2.5wt.% are performed (Fig. 3a). For 0.01 and 0.05wt.% ferrocene, only a thin layer of entangled nanotubes is observed. However, as soon as the ferrocene concentration reaches 0.1wt.%, the growth of a well-defined VACNT forest becomes effective with a growth rate as high as 20 µm/min, close to its maximum of 22 µm/min obtained with 0.25wt.% (Fig. 3b). For higher concentrations, the growth rate decreases to values in the 10-15 µm/min range. The trends are the same on the substrate located at the center of the furnace and on the reactor walls, with still mean values slightly lower for samples collected on the walls, due to variation along the reactor (Fig. S2). The VACNT carpet thickness increases linearly with the synthesis duration in the tested duration range up to 420 min, with a growth rate of 11.4 µm/min at 1.25wt.% and 2.5wt.% ferrocene (Fig. S3 in supplementary data).

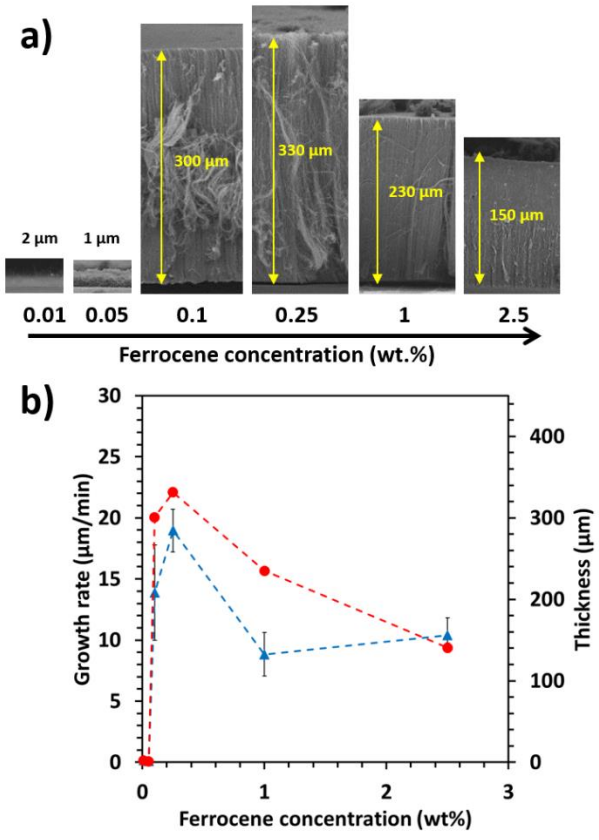

Fig. 3: Single injection. (a): SEM images of the VACNT carpets grown on the central substrate for increasing ferrocene concentration. (b): mean carpet thickness and growth rate on the central substrate (red dot) and on the reactor walls (blue triangle) as a function of ferrocene concentration. Dashed lines are added as eyes guide only. The thickness distribution was measured by SEM on the same samples with 20 measurement points for

the CNTs on the walls of the reactor and 3 measurement points for the CNTs on the substrate.

Therefore for this one-step aerosol assisted CCVD process operated at 800°C with hydrogen in the gas phase, the ferrocene concentration threshold allowing an efficient growth of VACNTs is as low as 0.1wt.%, while no growth at all was observed without hydrogen at 850°C for ferrocene concentration equal to 0.1 or 0.5wt% [15]. More generally, the present results represent a great improvement as compared to the state of the art related to the one-step CCVD process (Table 1) in terms of growth rate at very low ferrocene concentration.

3.2 Purity, diameter and structure of carbon nanotubes

The main characteristics of the VACNTs are similar regardless of the injection mode and depend only on the ferrocene concentration. Results obtained for the single injection mode will be discussed here and the ones regarding the double injection reported in Supplementary data.

Let's focus on single injection samples and compare SEM and TEM images of the formed nanotubes with 0.1wt.% and 2.5wt.% of ferrocene respectively (Fig. 4). The striking difference between both samples is in terms of cleanliness. At 0.1wt.%, the forest is very clean and no parasitic particles can be observed outside the nanotubes at the resolutions used for the observations. There are very few iron-based nanowires inside the nanotubes (Fig. 4a and 4c). The number of embedded Fe nanoparticles has been drastically reduced as compared to our previous results. Indeed, TEM micrographs on figure 4c) clearly indicate a high purity of CNT at low ferrocene concentration. On the contrary, at 2.5wt.% numerous iron-based particles exhibiting a nanowire shape are located inside the nanotubes (see also Fig. S4). In addition, a considerable amount of nanoparticles are located on CNT surface (Fig. 4b and 4d), as observed by others when the ferrocene concentration is high [19,21,33]. They are of varying sizes, some of them being encapsulated into carbon shells and some others giving rise to the growth of nanotubes of very small diameter which represent a low fraction of the sample mass and are not considered in the diameter distributions reported below. Such iron nanoparticles located on the CNT surface and the thin nanotubes observed on samples prepared with 2.5wt.% of ferrocene (Fig. 4d) cannot be detected in the sample obtained with 0.1wt.% of ferrocene (Fig. 4c). Therefore, lowering the ferrocene concentration induces a drastically reduction of the iron impurities inside the VACNT samples.

A detailed HRTEM analysis of a few individual nanotubes over their length (see Fig. S4) is used to characterize the iron-based nanowires found in the inner channel of the tubes. Their

average length and number density decrease significantly as the ferrocene concentration decreases. This detailed TEM analysis at higher magnification (Fig S4) shows also a highly reduced frequency of incorporation of nanowires into the tubes as well as a much lower mean size of these nanoparticles when the ferrocene concentration is reduced. Therefore, the amount of embedded nanoparticles is really low, and it is a great improvement for a one-step CCVD process. For 0.1wt.% ferrocene, only 2% of the length of the nanotube inner channel is occupied by iron nanowires, while it is 24% for 2.5wt.%. On average, it can be estimated that there is 1 nanowire every 2 µm at 0.1wt.% ferrocene while there is one nanowire every 0.4 µm at 2.5wt.% (See Table S2). An analysis of structural defects (corking) in the inner channel also shows a decrease in their occurrence for 0.1wt.% as compared to 2.5wt.%, but not in the same proportion as nanowires (Table S2).

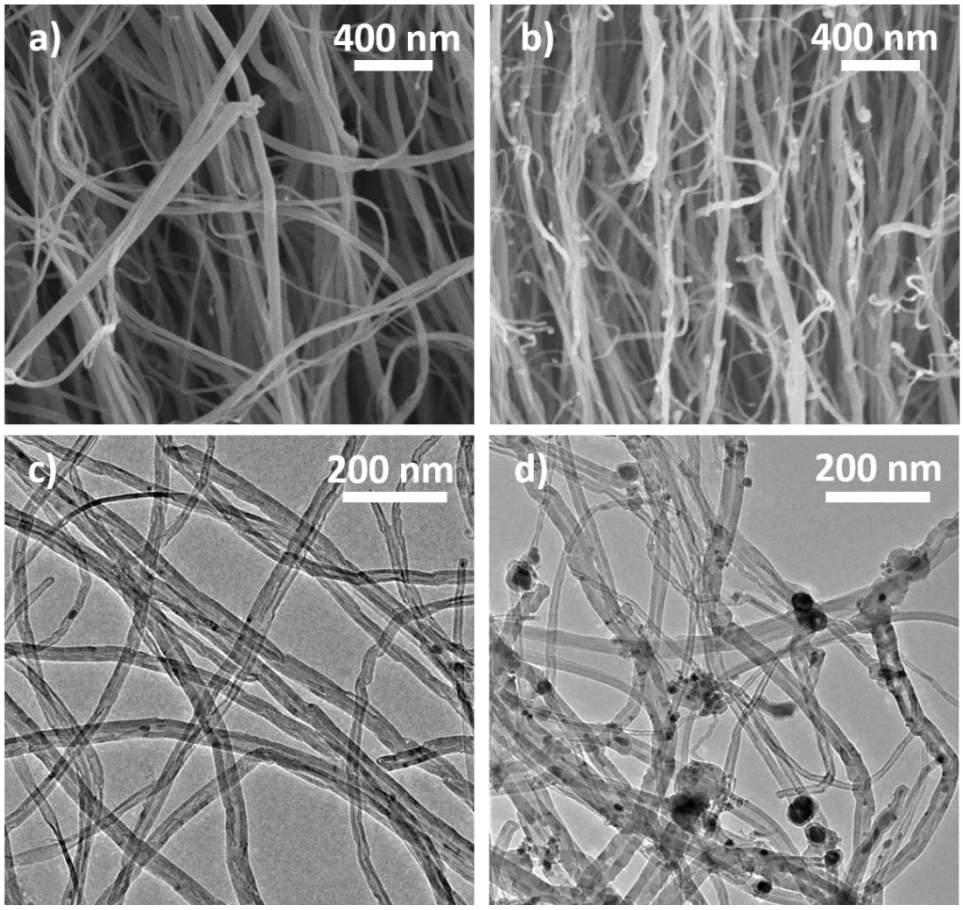

Fig. 4: Comparison in single injection between samples obtained with ferrocene concentration of 0.1 and 2.5wt.%. a) SEM image of 0.1%; b) SEM image of 2.5%; c) TEM image of 0.1%; and d) TEM image of 2.5%.

The iron content of VACNT forests is determined by TGA analysis under air (Fig. 5a) on samples taken in the same central area of the reactor as the ones used for the SEM and TEM

analysis above. In single injection, the iron content varies greatly and linearly with the ferrocene concentration, from 0.5wt.% at 0.1wt.% ferrocene up to 9wt.% at 2.5wt.% ferrocene. This value of 0.5 wt% of iron in VACNT sample is a remarkably low value as compared to the literature (see Table 1 and references herein) and is even lower than that of 0.56 recently published in a paper related to a two-step floating CCVD process[31]. It confirmed the great increase in the VACNT purity at low ferrocene concentration as observed by TEM above. In double injection, iron content variations are less pronounced as compared to single injection (Fig. 5a) due to the first injection sequence at 2.5wt.%. To verify that the variation in iron content with the ferrocene concentration is not due to a similar variation in iron chemical yield, we estimate the proportion of injected iron found in the final product. In single injection, the incorporated iron represents 40% of the injected iron at 0.1wt.% ferrocene and 50% at 2.5wt.%. Therefore, the incorporation rate of iron remains similar regardless of the ferrocene concentration and cannot be responsible for the high difference in iron content.

The catalytic yield (Fig. 5b) scales as the inverse of the ferrocene concentration for single injection. A very high and maximum catalytic yield about 200 (200g of carbon produced by iron gram) is obtained for the lowest concentration of ferrocene (0.1wt.%) and then decreases rapidly down to 10 when the ferrocene concentration increases. For double injection, the catalytic yield is varying in a slighter range, between 16 and 35, for the whole ferrocene concentration range.

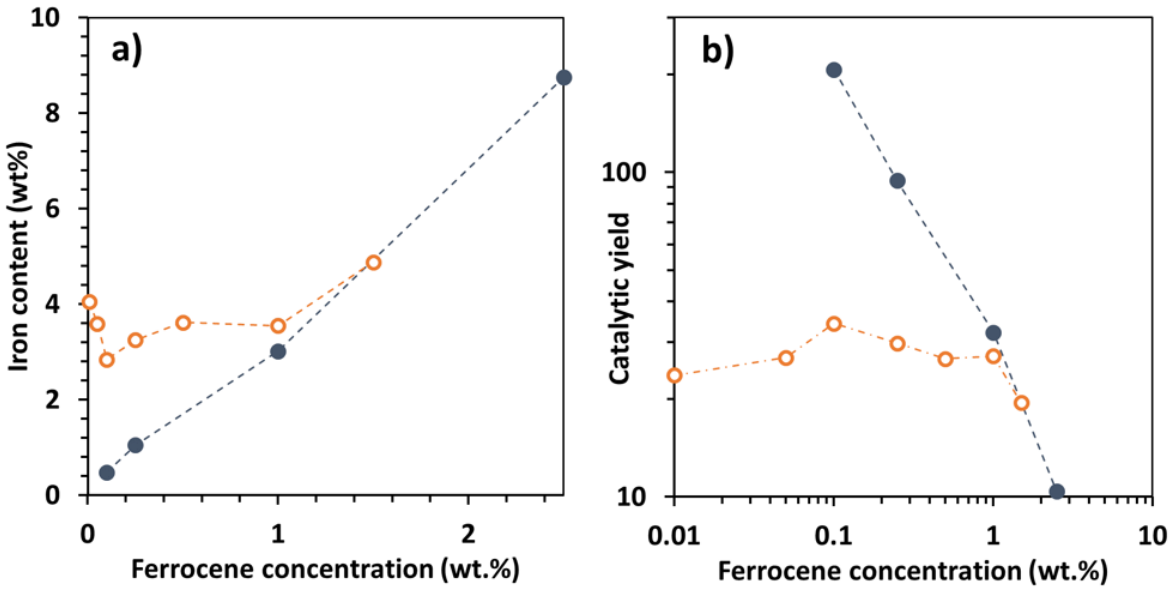

Fig. 5: Ferrocene concentration effect on a) iron content and b) catalytic yield, for single (full dot) and double (open dot) injection (in this last case, it is the ferrocene concentration of the second long injection sequence). Dashed lines are added as eyes guide only.

Regarding the CNT diameter, the distribution does not change with the ferrocene concentration (Fig. 6a), with external and internal average diameters around 35 nm and 9 nm respectively. Similar results are found in the case of double injection (Fig.S5). In terms of structural quality, the Raman spectra of the samples obtained with 0.1 and 2.5 w.t% ferrocene are compared in Fig. 6b (see Fig. S6 for double injection): G, D and D' bands at 1580 cm^{-1}, 1350 cm^{-1} and 1615 cm^{-1} respectively, as well as the 2D band at 2700 cm^{-1} are occurring. In multi-walled carbon nanotubes, the D band is associated with defects and disorder and is influenced by the curvature of the walls, while the G band is inherent to in plane tangential stretching of carbon-carbon bonds. The ratio between the D and G band intensities (I_D/I_G) is commonly used as a qualitative measure of the defect density in defective tubes: the higher this ratio, the lower the crystalline level [38,39]. This ratio is dependent on the excitation wavelength. The analysis of the Raman spectra recorded at 514 nm on the samples obtained in the current study gives rise to a I_D/I_G ratio remaining similar whatever the injection mode and the ferrocene concentration. This ratio is around 0.3 and the lowest value of 0.28 is obtained at 0.25wt.% ferrocene concentration in single injection (Table S1). Such values are low for multi-walled carbon nanotubes produced by CVD and are related to a low defect density as discussed by Meysami et al. [21]. These values compare well with those reported in Table 1 obtained with similar Raman wavelengths (514 or 532 nm) for samples formed in similar conditions in terms of carbon precursors and synthesis temperatures (750-850°C) [15,19,21]. By contrast, they are much lower than those reported in the range [0.56-0.79] by Kinoshita et al. [31] from synthesis at 700°C with acetylene as carbon source. However, it has been shown that the G band in CNT can be affected by defects [39], therefore as the 2D band does not represent a disorder-induced mode, the relative intensity of the D and 2D bands (I_D/I_{2D}) is also used as a qualitative measure of the defect density. Kinoshita el al. [31] found a I_D/I_{2D} ratio between 0.8 and 2. In the present work, this ratio is around 0.3 for almost all the ferrocene concentrations, apart for 2.5wt.% of ferrocene which gives rise to a ratio of 0.36. Such low I_D/I_{2D} ratio indicates a really good structural quality of the CNT forest that is well preserved and even slightly improved at low ferrocene concentration. This result corroborates the same trend observed by Cho *et al*. [20] and McKee *et al*. [19] with a similar one-step aerosol-assisted process.

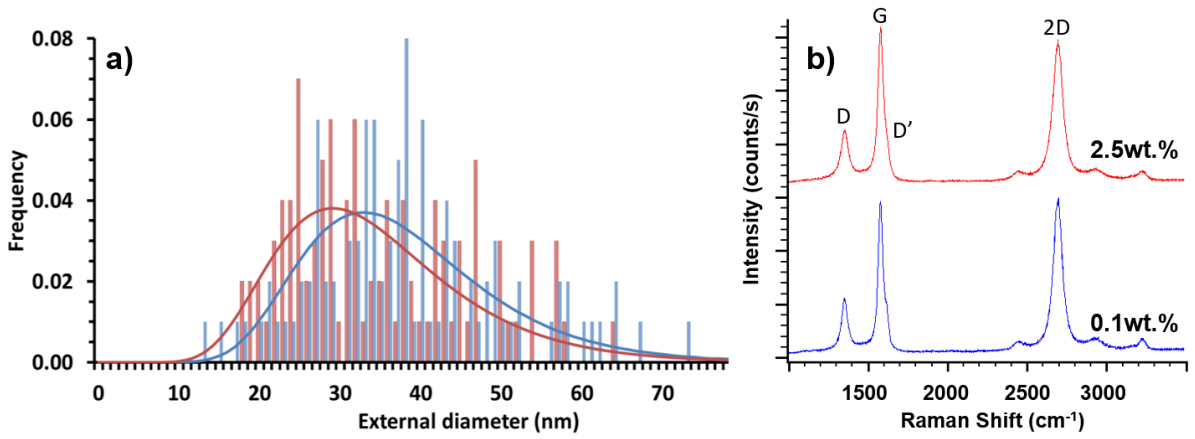

Fig. 6: Comparison in single injection between samples obtained with ferrocene concentration of 2.5 (red) and 0.1wt.% (blue), respectively. a) Nanotube external diameter distributions from the TEM analysis of more than 100 CNTs; b) Raman spectra acquired at 514 nm at the center of forest cross-sections.

3.3 VACNT forest density

The mass per unit area of VACNTs collected on the reactor walls in the oven center (Fig. 7a) increases with ferrocene concentration for both single and double injection experiments, meaning that the chemical yield improves in both cases. In single injection, the areal mass is close to 2mg/cm^2 at 0.1wt.% and then increases gradually up to 4 mg/cm^2. In double injection, the areal mass is already equal to 3 mg/cm^2 at 0.01wt.% ferrocene in the second injection and then rises up to more than 6 mg/cm^2, with values systematically higher than in single injection. The gap between the two curves remains approximately constant around 2.5 mg/cm^2 in excess in double injection as compared to single injection. This difference can be attributed to the effect of the first injection sequence with 2.5wt.% in the double injection mode. Reproducibility has been tested for experiments performed with ferrocene concentration of 0.1, 0.25 and 2.5 wt.% in single injection and 0.1, 0.25 and 0.5 wt.% in double injection. The observed deviations do not affect the general trends, particularly for single injection experiments (Fig. S6 in supplementary information).

From measurements of areal masses (Fig. 7a) and forest thicknesses (Fig. 2b and Fig. 3b), the forest density can be determined and increases with the ferrocene concentration, especially in single injection (Fig. 7b). Since nanotube diameters are similar whatever the ferrocene concentration, this density increase must be related to an increase in N, the number density of nanotubes (CNTs/cm^2). N can be estimated knowing the mean external diameter of the nanotubes and taking 1.8 g/cm^3 for the intrinsic carbon nanotube density as estimated by helium

picnometry. N is found about ~5 10^9 CNT/cm^2 at low ferrocene concentration, but reaches ~1.7 10^{10} CNT/cm^2 at 1wt.%. This result suggests that the number density of catalytic nanoparticles increases as well.

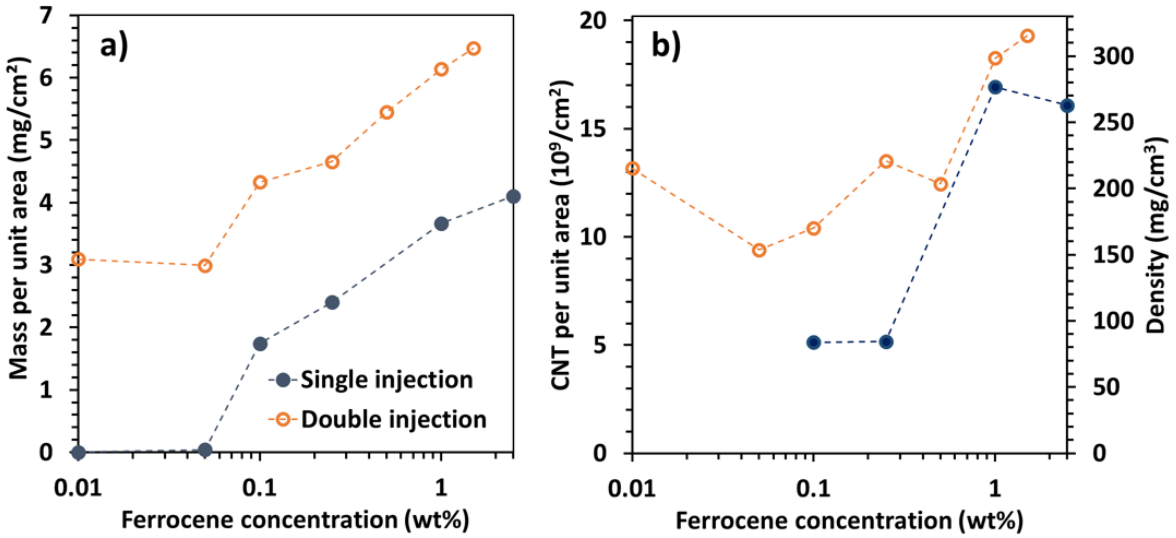

Fig. 7 – Ferrocene concentration effect on a) mass per unit area of carbon collected on the reactor walls in the center zone, and b) measured mass density, for single (full dot) and double (open dot) injection (in this last case, it is the ferrocene concentration of the second long injection sequence). Dashed lines are added as eyes guide only.

3.4 Oxidation resistance

The TGA mass-loss profiles are very dependent on the ferrocene concentration (Fig. 8a; see also Fig. S8). In single injection, the profile is strongly shifted towards the high temperatures when the ferrocene concentration decreases. The oxidation temperature (T_{ox}), taken as the temperature of the peak in the TGA graph derivatives (Fig. 8b and Fig. S8), decreases quasi-linearly from 685°C down to 550°C when ferrocene increases from 0.1 to 2.5wt.%. Since in single injection the iron content of the sample was previously found to be a linear function of the ferrocene concentration (Fig 5a), T_{ox} appears to be a linear function of the iron content as well (Fig. 8c and Fig. S9). In the case of double injection, the TGA profile exhibits a remarkable shoulder on the high temperature side when the ferrocene concentration in the second injection sequence is lower than 0.5wt.%, so that two T_{ox} (labelled Double1 and Double2) can be identified at low ferrocene concentrations (Fig. 8c and S9). The difference between both values is really significant (nearly 100°C) which points to the existence of two distinct components in the samples as discussed below.

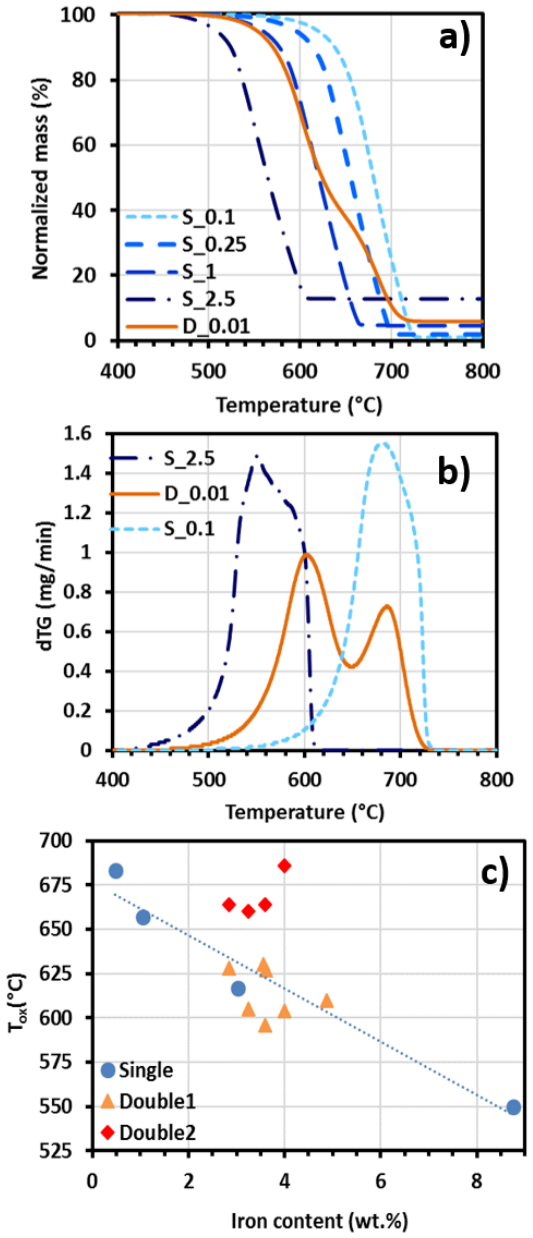

Fig. 8: a) TGA graphs obtained at a temperature rate of 10°C/min and b) their derivatives for single injection samples (blue dashed lines labelled from S_0.1 to S_2.5 according to the ferrocene concentration) compared to the double injection with 0.01wt.% ferrocene in the second injection sequence (orange solid line labelled D_0.01). c) Oxidation temperature as a function of iron content. In double injection the label "Double2" corresponds to the second peak at high temperature when observed in the dTG graph. See also Fig. S8.

4 Discussion

The present results show that the one-step aerosol-assisted CCVD process can be operated at very low ferrocene concentration (0.1 wt.%) using an Ar/H2 gas mixture as carrier gas. Using these conditions and a synthesis temperature of 800°C, we demonstrate that this one-step

process enables the formation with a high catalytic yield (200) of VACNT forests exhibiting low impurity level (0.5 wt.% of Fe). Such low ferrocene concentration does not involve any reduction of CNT growth rate since it remains higher than 20 µm/min. Compared to the literature (Table 1), it is, to our knowledge, the lowest concentration of ferrocene reported so far for aerosol-assisted CCVD process leading to such growth rates and impressive catalytic efficiency, thus involving the formation of high purity VACNT forests. The growth of a VACNT forest becomes impossible only when the ferrocene concentration falls below 0.1wt.%. When it increases up to 1wt.%, the growth rate decreases by a factor of 2, while the number density N is multiplied by more than 3 going from $5\ 10^9$ to $1.7\ 10^{10}$ cm^{-2}.

Regarding the mechanisms at play, hydrogen plays a significant role in the process of ferrocene decomposition. Indeed, our previous results obtained at 850°C with 2.5wt.% ferrocene [34] have shown that including 30% of H_2 in the Ar gas flow induces an increase of N from $5\ 10^9$ to $2\ 10^{10}$ $CNT.cm^{-2}$ as well as a decrease of the mean CNT external diameter. These results were attributed to the hydrogen induced enhancement of the dissociation rate of ferrocene. As a consequence, there is a fast rise of the iron partial pressure in the reactor and a high level of supersaturation which affects the homogeneous nucleation process of the iron nanoparticles. A much higher number of smaller nuclei forms, which leads to a higher number density of catalytic nanoparticles deposited on the substrate and therefore to a higher density of growing CNTs. Such very efficient effect of hydrogen on the catalytic particles density is responsible for the remarkable decrease in the ferrocene concentration allowing to reach the threshold in density of CNTs needed to form a self-supporting forest structure [40]. Interestingly, in the present work at 0.1wt.% ferrocene in single injection mode, N is equal to $5\ 10^9 CNT.cm^{-2}$, a value similar to the one obtained without hydrogen at 2.5wt.% ferrocene with the same one-step aerosol assisted CCVD process [18]. This number allowing the vertical self-organization of the interacting CNTs is comparable to the value of about $2\ 10^9$ $CNTs/cm^2$ reported by Bedewy *et al*. [40]. This threshold is obviously not reached below 0.1wt.%, explaining the absence of VACNT growth at such low concentration. This threshold was also not reached without hydrogen for ferrocene concentration below 1.25wt.%, explaining why no VACNTs were observed at 0.1 and 0.5wt.% by Castro et al. [15].

In double injection synthesis, the first injection sequence with 2.5wt.% ferrocene determines the density of catalytic nanoparticles. So N is higher from the beginning of the precursor injection and its evolution is less pronounced with the ferrocene concentration increase in the

second injection sequence, where a ferrocene concentration as low as 0.05wt.% is sufficient to sustain the growth.

The existence of a clear threshold in the ferrocene concentration allowing the self-organization of VACNTs is responsible for the sharp increase in the growth rate with ferrocene concentration observed for single injection experiments (Fig. 3b). The slow decrease observed after the maximum (Fig. 3b), as also observed by others [32,33], is generally attributed to an increase in VACNT density. Call *et al.* [41] show that ferrocene concentration dictates forest density but that forest thickness is limited by density presumably due to diffusion-limited precursor supply. However, in our case, the forest thickness is found proportional to the synthesis duration at least up to 90 min even at 1.25 wt.% ferrocene where the forest density is above 10^{10} CNT/cm^2 (Fig. S3). Indeed, the flow rate is too high and the average inter-tube distance too large (between 60 and 150 nm) to encounter feedstock resistance [42]. Same conclusion was reported by Cho *et al.* [20] leading them to invoke, as Bai *et al.* [33], a weaker activity of the catalytic nanoparticles due to their size increasing with ferrocene concentration [8]. However, in our study, the CNT diameter remains similar whatever the ferrocene concentration, which implies that the catalytic particle size remains also the same [8]. In the present range of ferrocene concentration, this size is mainly governed by temperature, H_2 content and nature of the substrate, all these parameters being constant here. On the other hand, when the number density of nanotubes increases, the amount of precursors available per nanotube decreases, in principle in inverse proportion to the density. This is not exactly what we are observing here since the mass per unit area that is the product of the two is not constant, but increases. Such result could be rationalized considering that at very low forest density, not all the carbon precursors impinging the substrate area around a given CNT (intertube distance is 150 nm) are able to interact with the catalyst particle, but their proportion increases when the intertube distance decreases. Such effect could explain the observed variation of growth rate.

Regarding the iron content of the VACNT forest, it increases linearly from 0.48 to 8.75 wt.% with the ferrocene concentration in single injection, and the atomic ratio Fe/C in the forest appears to be 10 times the Fe/C ratio in the precursors (Fig. S10). It means that the iron conversion is 10 times higher than the carbon conversion. It should be noted that the contribution of the catalyst nanoparticles themselves to the iron content is very low as is out of principle the case for any VACNT forest (see its estimation in Supplementary Data). The iron incorporated in the material is predominantly found as nanowires encapsulated in the inner channel as a consequence of the continuous refreshment of the catalyst nanoparticles from the

iron-based nanoparticles continuously nucleated in the gas phase [18] in the one-step aerosol-assisted CCVD process. When the ferrocene concentration is decreased, the percentage of the CNT inner channel length occupied by the nanowires (Fig. S4 and Table S2) drastically decreases: it is estimated to be 10 times lower for the optimal concentration of 0.1wt.% ferrocene as compared to 2.5wt.%, which corresponds to an encapsulation frequency which is 3 times lower.. Since the CNT growth rate is two-fold higher at 0.1wt.% than at 2.5 wt.%, it means that the acceleration in the refreshment at high ferrocene concentration does not allow to increase the growth rate but only leads to an increase of the iron content.

Iron can be incorporated in the forest also as nanoparticles found outside the nanotubes. This contribution increases a lot when the ferrocene concentration increases, as observed by SEM and TEM (Fig. 4) and by others [21,33]. Since TEM observations show that the amount of external nanoparticles is negligible in the sample obtained at 0.1wt.% ferrocene, then we can estimate from the TEM analysis of the inner channel (Table S2) that the iron inside the tubes represents about 2/3 of the total iron content for the sample formed with 2.5wt% ferrocene. Therefore, external nanoparticles contain at most a third of the iron content. Their presence in large quantities is due to the large increase, with the ferrocene concentration, of the number density of iron nanoparticles in the precursor gas flow going towards the substrate through the carpet. To avoid the formation of such large proportion of by-products in the presence of H_2, the ferrocene concentration must be kept lower than 1wt.%.

Regarding now the size and crystalline structure of the nanotubes, both TEM and Raman analysis show that their structure and diameter depend only slightly on the concentration of ferrocene in the range studied here. The ID/IG ratio of 0.3 indicates a good structural quality with a low defect density for MWCNTs as observed previously [15,21]. That is why it is not possible to interpret the large variation in the oxidation temperature with the ferrocene concentration in terms of variation of the structural properties. Even considering the position of the G-band, which was found to correlate with T_{ox} in the literature [43], it is not possible to invoke such structure evolution, since here, the G-band position is very stable (Table S1). Alternatively, the catalytic activity of the iron-based compounds inside the forests during the TGA was also considered in the literature since it is able to change the kinetic parameters of the oxidation [19,21,23–25]. In the present case, this second interpretation is strongly supported by the strong correlation found between T_{ox} and iron content in single injection synthesis (Fig.8c). Also, the highest oxidation temperature (680°C) obtained for the sample with the lowest iron content is found very similar to the one of VACNT sample freed from iron after a

heat-treatment at 2000°C [29]. Moreover, in double injection, the catalytic activity of the iron-based compounds allows to understand directly the presence of two components in the TGA graphs. When the ferrocene concentration is very different between the two injection sequences, two layers are formed with very different iron contents and different oxidation temperatures. The highest oxidation temperature is close to those obtained with single injection with a similar low ferrocene concentration. The large variation in oxidation temperature under dry air can be correlated to the iron content and the double peak observed for sample synthesized by double injection underlines the localized catalytic role of iron compounds in the oxidation reaction as mentioned in [25]. It could be used to perform selective oxidation of the carpet top in order to suppress the layer where the CNTs are entangled and to open the tubes. Also, double injection experiments offer the possibility to control independently forest density and growth rate while limiting the iron content. The forest density is determined by the ferrocene concentration in the first injection sequence while the growth rate depends mostly on the ferrocene concentration in the second injection sequence.

5 Conclusion

Our results show that, in the aerosol-assisted CCVD process, the addition of H_2 in the carrier gas results in a significant increase in the number density of catalytic nanoparticles, due to its strong influence on the decomposition kinetics of the ferrocene. As a result, the formation of a self-organized VACNT forest occurs at a much lower ferrocene concentration than without hydrogen and a pristine forest of high purity is formed with high catalytic yield at a performing growth rate. At 800°C, with 30% H_2 in Ar, VACNT forest is formed with only 0.1wt.% ferrocene (Fe/C=0.007at%), a value 25 times lower than the usual one of 2.5% optimized without hydrogen. The iron content falls down to 0.5wt.%, so that the catalytic yield is strongly enhanced by a factor of 20, while the growth rate is improved by a factor of 2 and the crystalline structure remains of high quality. A forest density of $5\ 10^9$ CNTs/cm^2 appears to be the threshold for the self-organization of the nanotubes to occur. This number density increases with the ferrocene concentration, due to the increase in the number density of catalytic nanoparticles. The iron content of the forest is directly proportional to the ferrocene concentration. When it decreases, the frequency of encapsulation of iron nanowires in the inner channel of the tubes decreases significantly and the oxidation resistance of the samples is greatly improved, with an increase in oxidation temperature equal to 100°C. Finally, double injection experiments appear to be an attractive approach in order to optimize independently the density and the growth rate of the forest, since the density is fixed by the initial ferrocene

concentration in the first short injection sequence while the growth rate can be controlled by the concentration in the second injection sequence.

Acknowledgement

The authors would like to thank M. Paternostre (CEA Saclay), P.-E. Coulon (LSI, Ecole Polytechnique Palaiseau) and J. N. Rouzaud (ENS Paris) for access to TEM, HRTEM and Raman analysis facilities, respectively.

Appendix A. Supplementary data

Supplementary data associated with this article can be found, in the online version, at

References

[1] A.M. Marconnet, N. Yamamoto, M.A. Panzer, B.L. Wardle, K.E. Goodson, Thermal Conduction in Aligned Carbon Nanotube- Polymer Nanocomposites with High Packing Density, ACS Nano. 5 (2011) 4818–4825. doi:10.1021/nn200847u.

[2] S. Lagoutte, P.-H. Aubert, M. Pinault, F.O. Tran-Van, M. Mayne-L 'hermite, C. Chevrot, Poly(3-methylthiophene)/Vertically Aligned Multi-walled Carbon Nanotubes: Electrochemical Synthesis, Characterizations and Electrochemical Storage Properties in Ionic Liquids, Electrochim. Acta. 130 (2014) 754–765. doi:10.1016/j.electacta.2014.03.097.

[3] K. Evanoff, J. Khan, A.A. Balandin, A. Magasinski, W.J. Ready, T.F. Fuller, G. Yushin, Towards ultrathick battery electrodes: Aligned carbon nanotube-enabled architecture, Adv. Mater. 24 (2012) 533–537. doi:10.1002/adma.201103044.

[4] H. Cebeci, I.Y. Stein, B.L. Wardle, Effect of nanofiber proximity on the mechanical behavior of high volume fraction aligned carbon nanotube arrays, Appl. Phys. Lett. 104 (2014). doi:10.1063/1.4862273.

[5] J.R. Raney, F. Fraternali, C. Daraio, Rate-independent dissipation and loading direction effects in compressed carbon nanotube arrays, Nanotechnology. 24 (2013) 255707. doi:10.1088/0957-4484/24/25/255707.

[6] M. Kumar, Y. Ando, Chemical Vapor Deposition of Carbon Nanotubes: A Review on Growth Mechanism and Mass Production, J. Nanosci. Nanotechnol. 10 (2010) 3739–

572 3758. doi:10.1166/jnn.2010.2939.

573 [7] R. Guzmán de Villoria, S.L. Figueredo, A.J. Hart, S.A.I. Steiner, A.H. Slocum, B.L.
574 Wardle, High-yield growth of vertically aligned carbon nanotubes on a continuously
575 moving substrate, Nanotechnology. 20 (2009) 405611. doi:10.1088/0957-
576 4484/20/40/405611.

577 [8] V. Jourdain, C. Bichara, Current understanding of the growth of carbon nanotubes in
578 catalytic chemical vapour deposition, Carbon N. Y. 58 (2013) 2–39.
579 doi:10.1016/j.carbon.2013.02.046.

580 [9] R. Andrews, D. Jacques, a. M. Rao, F. Derbyshire, D. Qian, X. Fan, E.C. Dickey, J.
581 Chen, Continuous production of aligned carbon nanotubes: a step closer to commercial
582 realization, Chem. Phys. Lett. 303 (1999) 467–474. doi:10.1016/S0009-2614(99)00282-
583 1.

584 [10] M. Mayne, N. Grobert, M. Terrones, R. Kamalakaran, M. Rühle, H.W. Kroto, D.R.M.
585 Walton, Pyrolytic production of aligned carbon nanotubes from homogeneously
586 dispersed benzene-based aerosols, Chem. Phys. Lett. 338 (2001) 101–107.
587 doi:10.1016/S0009-2614(01)00278-0.

588 [11] X. Zhang, a Cao, B. Wei, Y. Li, J. Wei, C. Xu, D. Wu, Rapid growth of well-aligned
589 carbon nanotube arrays, Chem. Phys. Lett. 362 (2002) 285–290. doi:10.1016/S0009-
590 2614(02)01025-4.

591 [12] R.A. Afre, T. Soga, T. Jimbo, M. Kumar, Y. Ando, M. Sharon, Growth of vertically
592 aligned carbon nanotubes on silicon and quartz substrate by spray pyrolysis of a natural
593 precursor: Turpentine oil, Chem. Phys. Lett. 414 (2005) 6–10.
594 doi:10.1016/j.cplett.2005.08.040.

595 [13] C. Singh, M.S.P. Shaffer, A.H. Windle, Production of controlled architectures of aligned
596 carbon nanotubes by an injection chemical vapour deposition method, Carbon N. Y. 41
597 (2003) 359–368.

598 [14] P. Boulanger, L. Belkadi, J. Descarpentries, D. Porterat, E. Hibert, A. Brouzes, M. Mille,
599 S. Patel, M. Pinault, C. Reynaud, M. Mayne-L'Hermite, J.M.M. Decamps, Towards
600 large scale aligned carbon nanotube composites: an industrial safe-by-design and
601 sustainable approach, J. Phys. Conf. Ser. 429 (2013) 012050. doi:10.1088/1742-
602 6596/429/1/012050.

603 [15] C. Castro, M. Pinault, S. Coste-Leconte, D. Porterat, N. Bendiab, C. Reynaud, M.
604 Mayne-L'Hermite, Dynamics of catalyst particle formation and multi-walled carbon
605 nanotube growth in aerosol-assisted catalytic chemical vapor deposition, Carbon N. Y.
606 48 (2010) 3807–3816. doi:10.1016/j.carbon.2010.06.045.

607 [16] M. Pinault, M. Mayne-L'Hermite, C. Reynaud, V. Pichot, P. Launois, D. Ballutaud, M.
608 Mayne-L'Hermite, C. Reynaud, V. Pichot, P. Launois, D. Ballutaud, Growth of
609 multiwalled carbon nanotubes during the initial stages of aerosol-assisted CCVD,
610 Carbon N. Y. 43 (2005) 2968–2976. doi:10.1016/j.carbon.2005.06.011.

611 [17] R. Xiang, G. Luo, W. Qian, Q. Zhang, Y. Wang, F. Wei, Q. Li, A. Cao, Encapsulation,
612 compensation, and substitution of catalyst particles during continuous growth of carbon
613 nanotubes, Adv. Mater. 19 (2007) 2360–2363. doi:10.1002/adma.200602468.

614 [18] P. Landois, M. Pinault, S. Rouzière, D. Porterat, C. Mocuta, E. Elkaim, M. Mayne-
615 L'Hermite, P. Launois, In situ time resolved wide angle X-ray diffraction study of
616 nanotube carpet growth: Nature of catalyst particles and progressive nanotube alignment,
617 Carbon N. Y. 87 (2015) 246–256. doi:10.1016/j.carbon.2015.01.046.

618 [19] G.S.B. McKee, C.P. Deck, K.S. Vecchio, Dimensional control of multi-walled carbon
619 nanotubes in floating-catalyst CVD synthesis, Carbon N. Y. 47 (2009) 2085–2094.
620 doi:10.1016/j.carbon.2009.03.060.

621 [20] J. Cho, A.R. Boccaccini, M.S.P. Shaffer, The influence of reagent stoichiometry on the
622 yield and aspect ratio of acid-oxidised injection CVD-grown multi-walled carbon
623 nanotubes, Carbon N. Y. 50 (2012) 3967–3976. doi:10.1016/j.carbon.2012.03.049.

624 [21] S.S. Meysami, A. a. Koós, F. Dillon, N. Grobert, Aerosol-assisted chemical vapour
625 deposition synthesis of multi-wall carbon nanotubes: II. An analytical study, Carbon N.
626 Y. 58 (2013) 151–158. doi:10.1016/j.carbon.2013.02.041.

627 [22] P.X. Hou, C. Liu, H.M. Cheng, Purification of carbon nanotubes, Carbon N. Y. 46 (2008)
628 2003–2025. doi:10.1016/j.carbon.2008.09.009.

629 [23] I.W. Chiang, B.E. Brinson, R.E. Smalley, J.L. Margrave, R.H. Hauge, Purification and
630 Characterization of Single-Wall Carbon Nanotubes, J. Phys. Chem. B. 105 (2001) 1157–
631 1161. doi:10.1021/jp003453z.

632 [24] A.-R. Leino, M. Mohl, J. Kukkola, P. Mäki-Arvela, T. Kokkonen, A. Shchukarev, K.
633 Kordas, Low-temperature catalytic oxidation of multi-walled carbon nanotubes, Carbon

N. Y. 57 (2013) 99–107. doi:10.1016/j.carbon.2013.01.040.

[25] C. Wang, S. Guo, X. Pan, W. Chen, X. Bao, Tailored cutting of carbon nanotubes and controlled dispersion of metal nanoparticles inside their channels, J. Mater. Chem. 18 (2008) 5782. doi:10.1039/b811560e.

[26] E.R. Edwards, E.F. Antunes, E.C. Botelho, M.R. Baldan, E.J. Corat, Evaluation of residual iron in carbon nanotubes purified by acid treatments, Appl. Surf. Sci. 258 (2011) 641–648. doi:10.1016/j.apsusc.2011.07.032.

[27] B.H.R. Suryanto, T. Fang, S. Cheong, R.D. Tilley, C. Zhao, From the inside-out: Leached metal impurities in multiwall carbon nanotubes for purification or electrocatalysis, J. Mater. Chem. A. 6 (2018) 4686–4694. doi:10.1039/c7ta11257b.

[28] X. Yang, M. Yang, H. Zhang, J. Zhao, X. Zhang, Q. Li, Electro-purification of carbon nanotube networks without damaging the assembly structure and crystallinity, Appl. Surf. Sci. 442 (2018) 232–238. doi:10.1016/j.apsusc.2018.02.169.

[29] M. Pinault, M. Mayne-L'Hermite, C. Reynaud, O. Beyssac, J.N. Rouzaud, C. Clinard, Carbon nanotubes produced by aerosol pyrolysis: growth mechanisms and post-annealing effects, Diam. Relat. Mater. 13 (2004) 1266–1269. doi:10.1016/j.diamond.2003.12.015.

[30] W. Huang, Y. Wang, G. Luo, F. Wei, 99.9% Purity Multi-Walled Carbon Nanotubes By Vacuum High-Temperature Annealing, Carbon N. Y. 41 (2003) 2585–2590. doi:10.1016/S0008-6223(03)00330-0.

[31] T. Kinoshita, M. Karita, T. Nakano, Y. Inoue, Two step floating catalyst chemical vapor deposition including in situ fabrication of catalyst nanoparticles and carbon nanotube forest growth with low impurity level, Carbon N. Y. 144 (2019) 152–160. doi:10.1016/j.carbon.2018.12.019.

[32] M.I. Ionescu, Y. Zhang, R. Li, X. Sun, H. Abou-Rachid, L.S. Lussier, Hydrogen-free spray pyrolysis chemical vapor deposition method for the carbon nanotube growth: Parametric studies, Appl. Surf. Sci. 257 (2011) 6843–6849. doi:10.1016/j.apsusc.2011.03.011.

[33] X. Bai, D. Li, Y. Wang, J. Liang, Effects of temperature and catalyst concentration on the growth of aligned carbon nanotubes, Tsinghua Sci. Technol. 10 (2005) 729–735. doi:10.1016/S1007-0214(05)70142-5.

[34] C. Castro, M. Pinault, D. Porterat, C. Reynaud, M. Mayne-L'Hermite, The role of hydrogen in the aerosol-assisted chemical vapor deposition process in producing thin and densely packed vertically aligned carbon nanotubes, Carbon N. Y. 61 (2013) 585–594. doi:10.1016/j.carbon.2013.05.040.

[35] M. Pinault, V. Pichot, H. Khodja, P. Launois, C. Reynaud, M. Mayne-L'Hermite, Evidence of sequential lift in growth of aligned multiwalled carbon nanotube multilayers, Nano Lett. 5 (2005) 2394–2398. doi:10.1021/nl051472k.

[36] S.S. Meysami, F. Dillon, A. a. Koós, Z. Aslam, N. Grobert, Aerosol-assisted chemical vapour deposition synthesis of multi-wall carbon nanotubes: I. Mapping the reactor, Carbon N. Y. 58 (2013) 159–169. doi:10.1016/j.carbon.2013.02.044.

[37] E. Charon, J.-N. Rouzaud, J. Aléon, Graphitization at low temperatures (600-1200°C) in the presence of iron implications in planetology, Carbon N. Y. 66 (2014) 178–190. doi:10.1016/j.carbon.2013.08.056.

[38] M.A. Pimenta, G. Dresselhaus, M.S. Dresselhaus, L.G. Cancado, A. Jorio, R. Saito, Studying disorder in graphite-based systems by Raman spectroscopy, Phys. Chem. Chem. Phys. 9 (2007) 1276–1291.

[39] J. Maultzsch, S. Reich, C. Thomsen, S. Webster, R. Czerw, D.L. Carroll, S.M.C. Vieira, P.R. Birkett, C.A. Rego, Raman characterization of boron-doped multiwalled carbon nanotubes, Appl. Phys. Lett. 81 (2002) 2647–2649. doi:10.1063/1.1512330.

[40] M. Bedewy, E.R. Meshot, H. Guo, E.A. Verploegen, W. Lu, A.J. Hart, Collective mechanism for the evolution and self-termination of vertically aligned carbon nanotube growth, J. Phys. Chem. C. 113 (2009) 20576–20582. doi:10.1021/jp904152v.

[41] R.W. Call, C.G. Read, C. Mart, T.C. Shen, The density factor in the synthesis of carbon nanotube forest by injection chemical vapor deposition, J. Appl. Phys. 112 (2012). doi:10.1063/1.4768928.

[42] R. Xiang, Z. Yang, Q. Zhang, G. Luo, W. Qian, F. Wei, M. Kadowaki, E. Einarsson, S. Maruyama, Growth deceleration of vertically aligned carbon nanotube arrays: Catalyst deactivation or feedstock diffusion controlled?, J. Phys. Chem. C. 112 (2008) 4892–4896. doi:10.1021/jp710730x.

[43] S. Santangelo, G. Messina, G. Faggio, M. Lanza, C. Milone, Evaluation of crystalline perfection degree of multi-walled carbon nanotubes: Correlations between thermal

696 kinetic analysis and micro-Raman spectroscopy, J. Raman Spectrosc. 42 (2011) 593–
697 602. doi:10.1002/jrs.2766.

698